FULL PAPER

Exploring the Origin of the Temperature-Dependent Behavior of PbS Nanocrystal Thin Films and Solar Cells

*Krisztina Szendrei, Mark Speirs, Widianta Gomulya, Dorota Jarzab, Marianna Manca, Oleksandr V. Mikhnenko, Maksym Yarema, Bart J. Kooi, Wolfgang Heiss, and Maria A. Loi**

Temperature-dependent studies of the electrical and optical properties of cross-linked PbS nanocrystal (NC) solar cells can provide deeper insight into their working mechanisms. It is demonstrated that the overall effect of temperature on the device efficiency originates from the temperature dependence of the open-circuit voltage and the short-circuit current, while the fill factor remains approximately constant. Extensive modeling provides signs of band-like transport in the inhomogeneously coupled NC active layer and shows that the charge transport is dominated by diffusion. Moreover, via low temperature absorption and photoluminescence (PL) measurements, it is shown that the optical properties of PbS thin films before and after benzenedithiol (BDT) treatment exhibit very distinct behavior. After BDT treatment, both the optical density (OD) and PL are shifted to lower energies, indicating the occurrence of electronic wave function overlap between adjacent NCs. Decrease of the temperature leads to additional red-shift of the OD and PL spectra, which is explained by the well-known temperature dependence of the PbS NCs' bandgap. Moreover, BDT treated PbS NCs show unusual properties, such as decrease of the PL signal and broadening of the spectra at low temperatures. These features can be attributed to the partial relaxation of the quantum confinement and the opening of new radiative and nonradiative pathways for recombination at lower temperatures due to the presence of trap states.

1. Introduction

The optical properties of semiconductor NCs exhibit strong size dependence due to the quantum confinement of the electronic wave functions. Due to these optical properties, NCs are considered to be very promising candidates both for optical and optoelectronic applications.[1,2] In particular, PbX (X = S, Se) NCs have emerged as solution-processable building blocks for device active layers, since they can access a greater portion of the near-infrared part of the solar spectrum, in contrast to most of the solution-processable organic polymers.[3,4] Besides the size and the shape of the NCs, the nature of the stabilizing ligands can also have large effects on the physical properties and, consequently, on device performance.[1,5–8] Modifying the surface properties of the NCs is inevitable for device applications, since most of the stabilizing ligands surrounding the NCs have an insulating nature. The active layer of NC based devices is generally prepared by layer-by-layer deposition of PbX particles followed by a solid-state ligand exchange using different short molecules such as thiols and amines.[9–14] As a result, the NCs form a disordered system where the features of both localized and coupled electronic states seem to coexist.[15] Recently, Talapin et al. reported band-like transport in NCs capped with the molecular metal chalcogenide complex $In_2Se_4^{2-}$.[16]

The difficulty of understanding the level of the delocalization of the electronic states in surface-modified PbX NC thin films lies in the fact that the charge-transport properties of these samples are not yet understood. Although, there are several studies focusing on transport properties of surface-modified PbX NC thin films used as active layers in field-effect transistors (FET) and solar cells, none of these is fully conclusive.[4,9,14–17] Few mechanisms have been proposed to try to explain charge separation and charge conduction in these NC-based devices. Choi et al. suggested that charge separation occurs via tunneling through a potential barrier without the aid of an external bias or potential gradient.[12] On the other hand, the free carrier transport following the charge separation is still to be explained. FET studies[9,15,18] suggest that long-range charge transport in NC solids occurs via a series of incoherent tunneling transitions between adjacent NCs, namely by nearest-neighbor hopping. This means that thousands of individual hops are required for

Dr. K. Szendrei, M. Speirs, W. Gomulya, Dr. D. Jarzab, M. Manca, O. V. Mikhnenko, Prof. B. J. Kooi, Prof. M. A. Loi
Zernike Institute for Advanced Materials
University of Groningen
Nijenborgh 4, Groningen, 9747 AG
The Netherlands
E-mail: M.A.Loi@rug.nl
M. Yarema, Prof. W. Heiss
Institute for Semiconductor and Solid State Physics
University of Linz
Altenbergerstr. 69, Linz, 4040, Austria

DOI: 10.1002/adfm.201102320

the free carriers to reach the electrodes. Tang et al.[19] and Luther et al.[4] reported a different mechanism in PbX Schottky solar cells, where the electron–hole pairs are separated by the built-in field followed by diffusion and drift of electrons and holes to the corresponding electrodes under the influence of the electric field. Due to uncertainties in the nature of the mechanism of the device functioning, further experimental and theoretical investigations are required for deeper understanding. Low-temperature studies on cross-linked PbX NC thin films could provide extra important information to understand the working mechanisms.

The temperature-dependent optical properties of NCs, stabilized by insulating organic ligands, have been extensively investigated in thin films providing the necessary basics for applications.[20–27] In general, it has been shown that reduced temperature can produce characteristic changes in the absorption and PL spectra, such as increasing of the intensity of the absorption and PL bands, reduction of the full-width-at-half-maximum (FWHM), changes in the number of bands and shifts of the absorption and PL maxima.

Nevertheless, to the best of our knowledge, there are no reports in the literature on the temperature-dependent absorption, PL, and current-voltage (*J–V*) characteristics of post-deposition ligand exchanged PbS NCs thin films. We believe that studying the temperature dependence of the electrical and optical properties of PbS NCs thin films can provide a better understanding of the device working mechanism and the physics of the cross-linked NC arrays.

2. Results and Discussion

2.1. Temperature Dependence of *J–V* Characteristics

We have recently reported the fabrication of PbS NC solar cells with record efficiencies.[28] Devices were fabricated similarly for this study, namely by spin-coating PbS NCs (with a bandgap of 1.1 eV) stabilized by insulating oleic acid (OA) ligands onto ITO patterned glass. The PbS NCs were treated with BDT to remove the insulating OA ligands and decrease the inter-particle distance (see TEM images in **Figure 1**b,c), thus inducing wave-function overlap and improving the charge transport in the PbS NC layer. The devices were completed by evaporation of 1 nm LiF and 100 nm Al on top of the active layer. To obtain more information about the charge transport properties, the temperature dependent *J–V* characteristics of surface modified PbS NC solar cells were measured under AM 1.5 illumination and in the dark (Figure 1a).

Figure 1 shows the obtained *J–V* characteristics under illumination at various temperatures. The overall effect of the temperature (*T*) on the device efficiency originates from the variation of the open-circuit voltage (V_{oc}) and the short-circuit

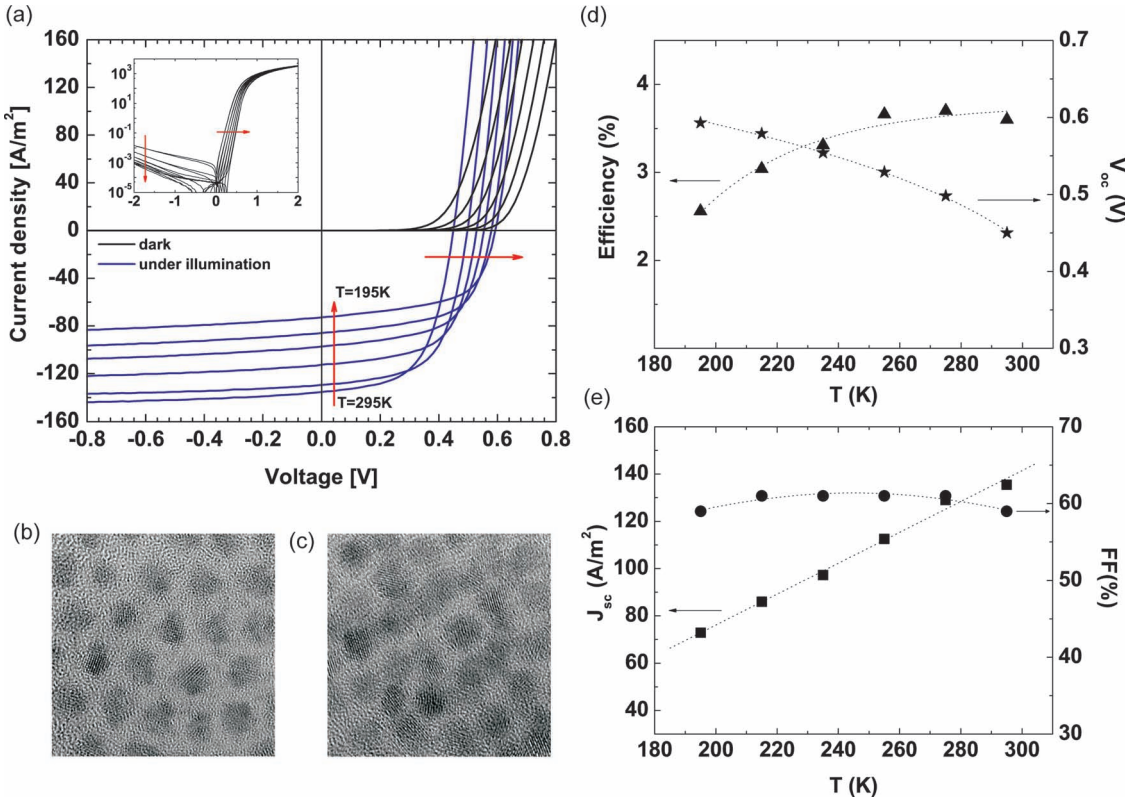

Figure 1. a) *J–V* characteristics of PbS NC solar cells under illumination from 293 to 195 K. Inset shows the *J–V* characteristics on a logarithmic scale in dark. b,c) TEM images (field of view 28.6 × 28.6 nm^2) of PbS NCs before (b), and after (c) ligand exchange. d,e) Experimental temperature dependence of the characteristic device parameters (J_{sc}, V_{oc}, *FF*, and efficiency).

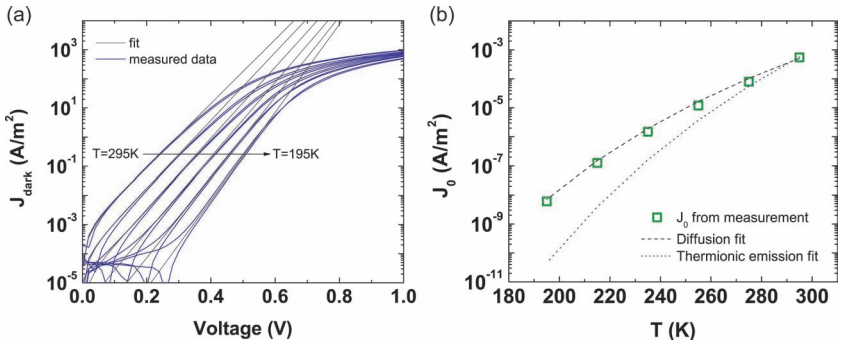

Figure 2. a) Dark *J–V* characteristics of PbS NC solar cells. b) Temperature dependence of the J_0 modeled by using diffusion and thermionic emission theory.

current (J_{sc}). The net effect is that the V_{oc} increases and the J_{sc} decreases with decreasing temperature, while the fill factor (*FF*) remains approximately constant. A similar effect can be observed for Si solar cells[29] due to the decreasing number of thermally generated carriers in the cell; however, the decrease of the J_{sc} is much smaller than in our experiments. In organic solar cells, which are characterized by hopping-like transport, losses in the *FF* also contribute to the decrease of the device efficiency besides the strong decrease of the J_{sc}, owing to the reduced carrier mobilities at lower temperatures.[30,31]

The *J–V* characteristics of a Schottky solar cell under illumination can be described by the following equation:[32]

$$J = J_0 \left[\exp\left(\frac{qV}{nkT}\right) - 1 \right] - J_{ph} \quad (1)$$

where J is the output current density, J_0 is the reverse saturation current density, q is the elementary charge, V is the voltage across the cell, n is the ideality factor, k is the Boltzmann constant, T is the temperature, and J_{ph} is the generated photocurrent density. At open circuit voltage (V_{oc}) the output current density $J = 0$, therefore Equation 1 can be simplified and the V_{oc} can be expressed as:

$$V_{oc} = \frac{nkT}{q} \ln\left(\frac{J_{ph}}{J_0}\right) \quad (2)$$

The temperature affects J (Equation 1) directly by means of the exponential term and indirectly via J_0. Clearly, a decrease in T increases the value of the exponent in Equation 1, while a reduction of T results in lower values of the J_0, which will be shown later on (**Figure 2**b). The net effect will be to increase the V_{oc} with decreasing temperature. As we have mentioned, the reduction in the J_{sc} of PbS NC solar cells with decreasing temperature is much more pronounced than in Si solar cells. The number of generated carriers is drastically decreased from 295 to 195 K, which could be due to hindered mobility and more specifically an increase of carrier trapping by surface defects.

In contrast, the *FF* of the PbS NC devices stays approximately constant, as can be seen in Figure 1d, where the *FF* is plotted together with the other characteristic parameters against the temperature (Figure 1b–e). In general, it can be concluded, that the device efficiency slightly increases when the T is decreased from 293 to 255 K, since the increase in the V_{oc} is larger than the decrease in the J_{sc}. However, below 255 K the decrease in the J_{sc} becomes dominating and the efficiency decreases (Figure 1e). HR–TEM (high-resolution transmission electron microscopy) images depicted in Figures 1b and c illustrate the reduction of the inter-particle spacing after BDT treatment. The separation between the surfaces of adjacent NCs can be estimated as approximately 2 nm with OA passivation. While after BDT treatment this distance decreases to approximately 0.5 nm, which is in close agreement with other literature data.[12] However, the distribution of coupling distances is inhomogeneous; some of the NCs seem more strongly coupled than others which has important consequences on the charge transport properties of the NC thin films. This idea is further supported by low temperature optical measurements on BDT treated PbS NC thin films to be shown later.

The temperature dependence of the V_{oc} of the PbS solar cells (Figure 1d) can be analytically modeled by using the extracted values of the J_0 at different temperatures. The values of J_0 cannot be directly measured, but they can be determined from the temperature-dependent *J–V* characteristics of the solar cells measured in the dark (Figure 2a).

By fitting the exponential part of the *J–V* characteristics to the Shockley diode equation (Equation 3):

$$J = J_0 \left[\exp\left(\frac{qV}{nkT}\right) - 1 \right] \quad (3)$$

the two fit parameters J_0 and n can be determined.[32] The obtained saturation current density J_0 as a function of temperature is plotted in Figure 2b and it can be modeled by using two existing theories. The first theory is the so-called thermionic emission theory. This theory assumes that only carriers with energy larger than the barrier height (φ_B) at the metal–semiconductor interface can contribute to the current flow and the shape of the barrier profile can be neglected. The current density can be expressed as:[32]

$$J = AT^2 \exp\left(-\frac{q\phi_B}{kT}\right) \left[\exp\left(\frac{qV}{kT}\right) - 1 \right] \quad (4)$$

where $A = 4\pi m^* k^2/h^3$ is the Richardson constant and ϕ_B is the barrier height. In the expression of the Richardson constant m^* is the effective mass of the charge carriers, and h is the Planck constant.

The second theory is the so-called diffusion theory, where the driving force, which is distributed over the whole length of the depletion layer, is the difference in carrier concentration. Hence, the current is limited by diffusion (similarly to that of a bulk semiconductor or a p–n junction), rather than by the barrier height. The current in this case is given by:[32]

$$J = qN_c D \left[\exp\left(\frac{qV}{kT}\right) - 1 \right] \Big/ \int_0^{W_D} \exp\left[\frac{E_c(x)}{kT}\right] dx \quad (5)$$

where N_V is the effective density of states in the valence band edge, D is the diffusion coefficient, W_D is the depletion width,

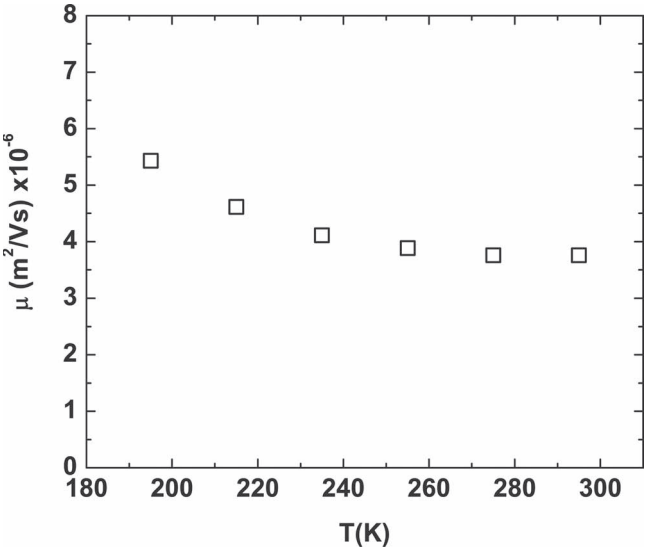

Figure 3. Temperature dependence of the calculated mobility, obtained from the Einstein relation.

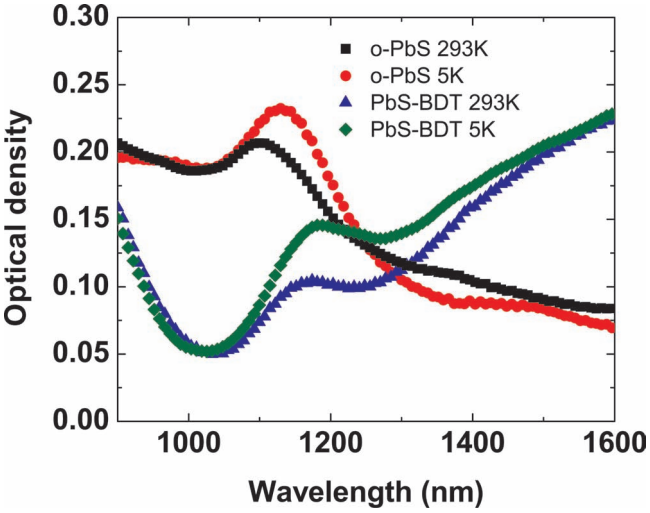

Figure 4. Comparison of the temperature dependent absorption spectra of PbS NCs before and after BDT treatment.

and E_V is the valence band edge. Assuming full depletion of our devices[4] and a triangularly shaped barrier, Equation 5 can be modified and the current density can be expressed as:

$$J = \frac{A^* \sqrt{T} \phi_B}{\exp\left(\frac{q\phi_B}{kT}\right) - 1} \left[\exp\left(\frac{qV}{kT}\right) - 1\right] \quad (6)$$

where $A^* = d^2 N_c D)/dk$, where d is the device thickness and $N_c = 2\left(\frac{2\pi m^* kT}{h^2}\right)^{3/2}$. We used Equation 4 and 6 to predict the values of the J_0 (Figure 2b). The thermionic emission model predicts two orders of magnitude lower J_0 at lower temperatures. Note that independently of the barrier height used in the model, the fit never agrees with the experimental data, since the slope of the J_0 does not change. Conversely, the diffusion theory provides a perfect agreement with experimental data (see Figure 2b). These observations are consistent with previous reports on Schottky barriers in Al/PbS junctions[33] and other low mobility semiconductors.[34] Moreover, the fitting process of the J_0 allows the direct extraction of the barrier height φ_B. The calculated value of the barrier height from Equation 6 is φ_B = 0.545 eV, which is in good agreement with previously reported experimental data.[35] When fixing this experimental value in Equation 6, the diffusion coefficients (D) can be extracted by fitting to Equation 6. The extracted diffusion coefficients are used to calculate the carrier mobilities (μ) with the Einstein relation ($\mu = D/kT$) at different temperatures. The calculated mobility (shown in **Figure 3**) depends weakly on temperature but shows a slight increase with decreasing temperature. This behavior is in contradiction with a hopping-based transport mechanism, since in that case the mobility and the FF should decrease with temperature.[18,36–38] However, disorder effects due to the varying degrees of coupling in the active layer (Figure 1c) preclude assignment to a specific mechanism, indicating more complex charge transport mechanisms (including the combination of hopping and band-like transport). It is noteworthy that signs of band-like transport were recently revealed in NCs capped with a metal chalcogenide complex showing similar increase in carrier mobility with decreasing temperature.[16]

2.2. Temperature Dependence of the Optical Properties

2.2.1. Temperature Dependent Absorption

Information about the degree of wave function overlap between NCs and the presence of trap states can be obtained also with optical measurements such as absorption and photoluminescence spectroscopy. The temperature dependence of the absorption (optical density (OD)) of oleic acid stabilized PbS NCs (o-PbS) has already been studied by other authors.[20,21] A typical experimental dataset of the temperature dependent OD of drop casted PbS NCs is shown in **Figure 4**. As can be seen, the absorption of the first excitonic peak of the PbS NCs is at around 1100 nm at 293 K. With decreasing temperature the spectra shows a red-shift and the intensity of the first excitonic peak increases. At 5 K the first excitonic peak is red-shifted to approximately 1130 nm. This red-shift of the OD spectra is related to the temperature dependence of the energy bandgap (E_g) of PbS, namely that E_g decreases with decreasing temperature.

The variation of the NCs bandgap with temperature can be characterized by the temperature coefficient (dE_g/dT)[39] which depends strongly on the NC size.[20] The value of dE_g/dT was determined according to the literature[27] and calculated to be 104 μeV K^{-1}. This extracted value of the temperature coefficient is in agreement with prior published data.[20]

Figure 4 also shows the OD spectra of PbS NCs measured at different temperatures after cross-linking with BDT molecules (PbS-BDT). The first excitonic peak at 293 K is located at around 1170 nm and is red-shifted by approximately 15 nm at 5 K. At this temperature the oscillator strength of the excitonic transition increases due to the lower electron–phonon interaction. In addition, a broad band appears from around 1280 nm and onwards, which can be attributed either to the wave function

overlaps and/or to the appearance of defect states as a result of the cross-linking process. Drude-type absorption[40] also could be the reason for the spectral broadening; this could eventually be ruled out by measuring the optical density further down to the infrared. Note, that this broadening cannot be observed in the IPCE spectrum,[28] indicating that the absorption from this region does not contribute to the photocurrent. This experimental observation agrees with the presence of defect states on the NCs' surface. The broadening of the spectra above the first excitonic peak after EDT treatment has been illustrated in several studies, however, without any comment on the underlying physical reason.[4,19]

The comparison between the OD of o-PbS and PbS-BDT at 293 and 5 K shows that the transition assigned to the first excitonic peak of PbS NCs is still evident, but the peak is red-shifted by 70 nm after BDT treatment (from 1100 to 1170 nm) and by another 55 nm when the sample is measured at 5 K. Moreover, the absorption peak is broadened and has a lower intensity with respect to the NCs stabilized by oleic acid ligands as a result of the surface modification. When PbS NCs are stabilized by oleic acid ligands, the electron and hole wave functions are localized on the individual NCs. In contrast, after BDT treatment the NCs are pulled closer together, resulting in a hybrid situation where the wave functions remain partly localized, accounting for the excitonic absorption, while some start to spill-out and couple, relaxing the quantum confinement.[1] As a consequence, the partial delocalization of the excitons occurs over several NCs. The additional red-shift of the PbS-BDT absorption with decreasing temperature can be explained by the thermal expansion, as has been mentioned above.

Since in PbS-BDT NC thin films the transition of the first excitonic peak is still present but is accompanied by spectral broadening and shift of the absorption, we believe that our thin films are composed of inhomogeneously coupled NCs which leads to complex charge transport mechanisms (including band-like transport).[41] For optoelectronics, the ultimate goal would be to design NCs maintaining a certain amount of optical confinement in combination with strong coupling, which would result in bulk-like transport properties.

2.2.2. Temperature-Dependent Steady-State Photoluminescence

Similar to the absorption behavior, the PL spectra of o-PbS NCs and PbS-BDT exhibit a strong temperature dependence as well. The experimental dataset of the steady-state PL spectra of the o-PbS NCs thin films at different temperatures is presented in **Figure 5**a. The PL of o-PbS NCs at 293 K shows a maximum at 1242 nm and a red-shift to 1346 nm with decreasing temperature. In addition to the red-shift, the full-width at half maximum (FWHM) of the PL peak at low temperatures decreases to 46% of its original value (the PL maxima and FWHM values are determined from Gaussian fits of the PL spectra at different temperatures). Moreover, the PL intensity increases with decreasing temperature by more than a factor of four.

The red-shift can easily be explained by the thermal expansion discussed above. The decrease of the FWHM and the increase of the PL intensity with decreasing temperature are due to the suppression of the phonon-coupled quenching of

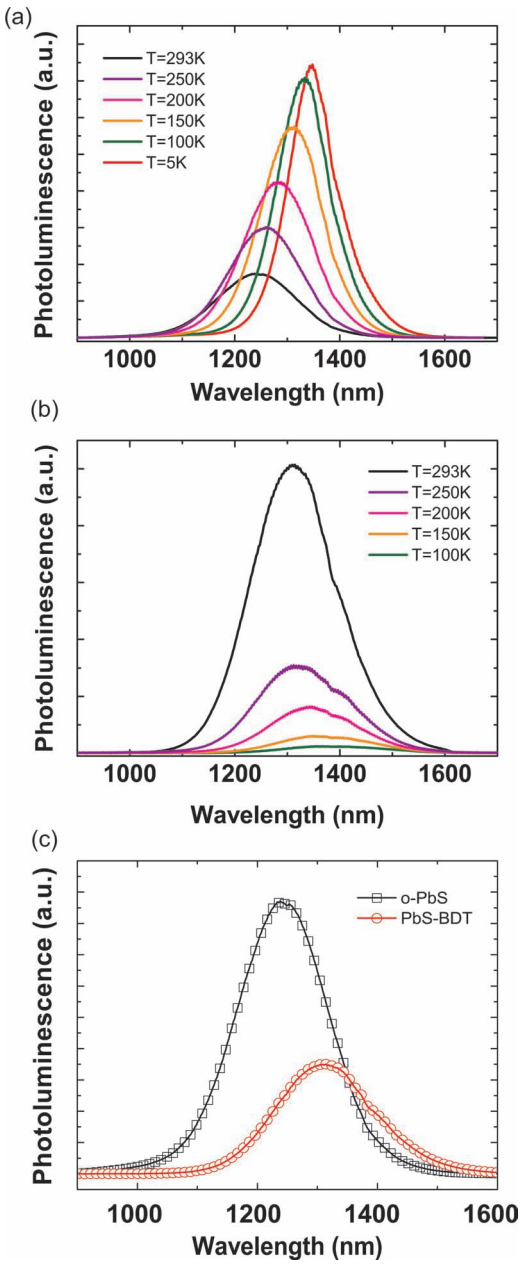

Figure 5. Steady-state PL spectra of: a) o-PbS NCs, and, b) PbS-BDT at different temperatures. c) Comparison of the steady-state PL spectra of the o-PbS NCs and PbS-BDT at 293 K.

the excitons. In detail, the probability of the electron–phonon scattering decreases due to the reduced number of lattice vibrations (phonons) at lower temperatures. Similar narrowing of the PL spectra of PbX NCs has also been observed in several works.[25,42,43]

In contrast, after surface modification of o-PbS NCs with BDT molecules, the PL of the NCs becomes more complex and shows peculiar characteristics. The PL of PbS-BDT at 293 K shifts towards the red, becomes more broad and the intensity of the PL is quenched with respect to the PL of o-PbS NCs, as illustrated in Figure 5c. The observed red-shift respect to the

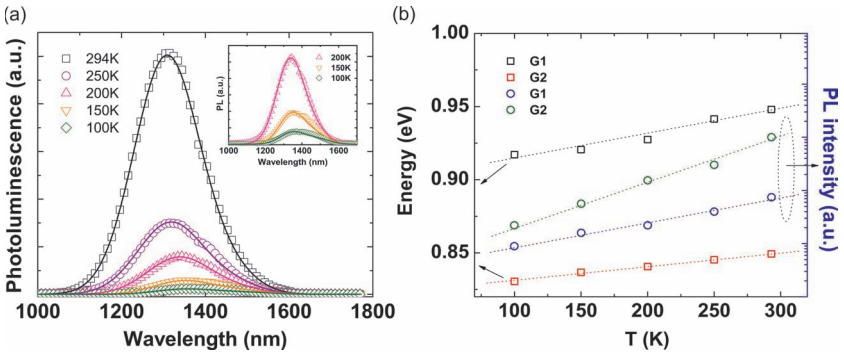

Figure 6. a) Gaussian fits of the steady-state PL of PbS-BDT at different temperatures. Inset shows the Gaussian fits at lower temperatures. b) Temperature dependence of the PL peak energy (□) and peak intensity (○) as obtained from the Gaussian fits.

o-PbS can be attributed to variation of the average dielectric constant of the film upon ligand exchange.[44]

By decreasing the temperature, an additional red-shift occurs (see Figure 5b and **Figure 6**a), similarly to what has been revealed for the PL of o-PbS NCs, due to the thermal expansion phenomenon. However, instead of the PL enhancement, we observed PL quenching at lower temperatures as well as the appearance of broadening of the excitonic emission. The increase of the PL with increasing temperature is unexpected due to the stronger importance of the electron-phonon interactions. The observed lowering of the intensity at low temperature can be due to nonradiative processes coming into play through trapping of the excitons. There are strikingly few reports discussing the temperature anti-quenching of the PL in semiconducting NCs. Wuister et al. investigated the temperature anti-quenching of PL in CdSe and CdTe NCs and indicated that the surface passivation decreases with temperature due to the phase transition of the capping ligands and displacements of the surface atoms.[45,46]

The role of the coordinating ligands around the NCs concerns not only the stabilization in solution and confinement of the charge carriers inside the NCs, but also the passivation of the dangling lone electron pairs of the surface atoms (Pb and S). The spatial confinement is very sensitive to surface–ligand interaction and subtle changes in the nature of the stabilizing ligands can increase or decrease the PL quantum efficiency.[7,47–49] Insufficient passivation of the NCs' surface leads to the appearance of defect states, which can create radiative and nonradiative pathways for recombination of the excitons.[48–51] For instance, Pb dangling bonds can introduce shallow donor states close to the conduction band edge, while dangling bonds of S atoms can create acceptor states in the middle of the bandgap of PbS NCs.[52] Bryant and Jaskolski reported similar observations on passivated and unpassivated CdS NCs.[53]

In addition, if the distance between adjacent NCs decreases, the confinement of charge carriers relaxes causing also a decrease of the PL. To sum up, due to relaxation of the quantum confinement and the reduction of surface passivation the excitonic emission of the NCs is quenched and the spectral shape is modified due to emerging transitions, originating from new states located in the NCs' bandgap.

To gain deeper insight into the experimental results, the PL spectra of PbS-BDT at different temperatures were fitted by using two Gaussian curves. It is important to notice that the main dip at around 1380 nm (Figure 6) most probably originates from the absorption of water molecules being present in the optical path; therefore is neglected during the analysis. The sum of the two Gaussians provides a good fit to the experimental data, as shown in Figure 6a. The Gaussian fits at lower temperatures are shown for clarity as an inset of Figure 6a. The parameters extracted from the Gaussian analysis are illustrated in Figure 6b, where black and red squares represent the temperature dependence of the Gaussian peak energy. Gaussian 1 (G1) is attributed to the excitonic emission while G2 is related to trap and/or impurity-associated transitions. It is interesting to note that G2 shows a similar trend to G1 with decreasing temperature, suggesting a strict correlation with the excitonic transition and the bandgap of the NCs. The presence of this state is not evidenced in the o-PbS samples which could be due to the fact that the emission intensity of o-PbS is much stronger than the one of PbS-BDT, covering the emission from this defect-related state.

Green and blue circles in Figure 6b illustrate how the PL intensities of the two Gaussians change with temperature. As can be seen, G1 and G2 are quenched in different proportion by decreasing the temperature. The decrease of the excitonic emission with decreasing temperature can be explained by the depopulation of the excitonic levels through trap states with consequent opening of nonradiative pathways in combination with the trap-associated transition. We suggest that G2 originates from impurity and/or Pb dangling bond-induced defect states, while S dangling bonds introduce midgap states serving as nonradiative quenching centers.

Charge carrier losses through defect related states could also explain the decrease of J_{sc} with decreasing temperature in our NC solar cells and the pinning of the Fermi level of the cathode metal observed by changing the electrode metal.

2.2.3. Dynamics of the Photoluminescence

The study of the PL dynamics can provide additional information on the recombination of the photoinduced excitations. **Figure 7**a and b illustrate the PL decay at 293 K before and after surface modification, respectively. The PL decay of o-PbS NCs shows a mono-exponential decay with a time constant of approximately 35 ns, while after BDT treatment the decay becomes bi-exponential with a slower component of around 2.5 ns and a faster component of approximately 203 ps. It is important to notice that different values (ranging from microseconds to the tens of nanoseconds) are reported in the literature for dynamics of the photoluminescence of NCs thin films.[54–57] The dissimilarities between these values are ascribed to the nature of the ligands, size of the NCs and the thin film organization. Most importantly, the bi-exponential behavior of BDT-treated samples and the shorter lifetime can be attributed to several phenomena:

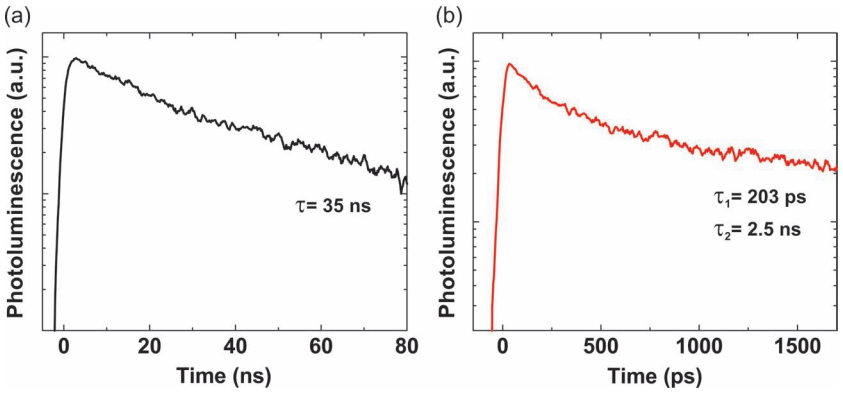

Figure 7. PL decay of: a) o-PbS, and, b) PbS-BDT at 293 K.

i) depopulation of the excitonic level and transfer to the defect states, and, ii) partial relaxation of the quantum confinement.

3. Conclusions

We sought to explain the physics of PbS NC solar cells by means of their temperature dependence. We have demonstrated that the overall effect of the temperature on the device efficiency originates from the temperature dependence of V_{oc} and J_{sc}. The net effect is that the V_{oc} increases and J_{sc} decreases with decreasing temperature, while the *FF* remains approximately constant. The temperature dependence of the V_{oc} of the PbS solar cells was successfully modeled by using the extracted values of the J_0 at different temperatures. The thermionic emission model predicted two orders of magnitude lower J_0 at lower temperatures than the diffusion theory, which provided perfect agreement to the experimental data.

The optical density (OD) of PbS films after BDT treatment shows that the first excitonic peak is red-shifted with respect to the absorption of o-PbS films and a broad band appears from approximately 1280 nm and onwards, which can be attributed either to the wave function overlaps and/or to the appearance of defect states as a result of the cross-linking process.

Since the first excitonic peak is still present in the OD spectra of PbS-BDT NC thin films together with the spectral broadening, we suggest that the device active layer is composed of inhomogenously coupled NCs, which leads to complex charge transport mechanisms including band-like transport.

Similarly to the absorption behavior, the PL spectra of o-PbS NCs and PbS-BDT also exhibit strong temperature dependence. At lower temperatures the PL of o-PbS NCs is red-shifted, its intensity is increased and the FWHM of the PL spectra decreased to 46% of its original value. In contrast, the PL of PbS-BDT exhibit quenched PL, indicating wave function overlaps and the opening of new nonradiative pathways at lower temperatures mediated by trapping of the excitons through defect states. This is supported by an analysis of the PL spectra of the PbS-BDT at different temperatures, based on Gaussian fits to the experimental data.

The comparison of the PL decay of o-PbS NCs and PbS-BDT also confirms the delocalization of the wave functions and the presence of nonradiative processes.

Finally, the presence of trap states in the active layer is at the moment a limiting factor in the performance of the NC solar cells. Future efforts in controlling and reducing the number of trap states may result in the fabrication of more efficient solar cells.

4. Experimental Section

For low temperature *J–V* measurements PbS NC solar cells were prepared as reported in the literature.[28] Current–voltage characteristics were recorded at different temperatures using a Keithley 2400 SourceMeter in a nitrogen filled glove-box. The desired temperatures were obtained by cooling the metal holder of the solar cells with liquid nitrogen. Measurements were performed in the dark and under illumination from a Steuernagel SolarConstant 1200 metal halide lamp calibrated to 1 Sun intensity and corrected for spectral mismatch with the AM1.5G spectrum using a Si reference cell.

High-resolution TEM images were recorded using a JEOL 2010F operating at 200 kV. The 512 pixels × 512 pixels images presented here show a field of view of 28.6 × 28.6 nm^2.

Low-temperature optical density measurements were performed by using an absorption setup consisting of a Tungsten lamp, a continuous flow helium cryostat (He-flux- Oxford Optistat), a monochromator and an Andor InGaAs photodiode array detector.

For low-temperature steady-state and time-resolved PL measurements, the samples were prepared on quartz substrates and loaded into the same He-flux cryostat. The samples were excited at approximately 380 nm by the second harmonic of a mode-locked Ti:Sapphire laser delivering pulses with a pulse duration of 150 fs. To vary the repetition rate of the exciting pulses, an optical pulse selector was used. Time-resolved traces were recorded with a NIR sensitive Hamamatsu streak camera working in single sweep mode. The steady-state PL spectra in the near-infrared were obtained with an InGaAs detector from Andor. The PL spectra were corrected for the spectral response of the setup using a calibrated light source.

Acknowledgements

Financial support from the European Commission through the Human Potential Programs (RTN Nanomatch, Contract No. MRTN-CT-2006-035884) and from the Austrian Science Fund FWF (Project SFB-IRON) is gratefully acknowledged. The authors thank R. A. J. Janssen, P. W. M. Blom, and T. Banerjee for discussions and J. Harkema, F. van der Horst, and A. Kamp for technical support. K.S. thanks P. de Bruyn for fruitful discussions and helping in the modeling.

Received: September 28, 2011
Revised: November 29, 2011
Published online: February 2, 2012

[1] D. V. Talapin, J.-S. Lee, M. V. Kovalenko, E. V. Shevchenko, *Chem. Rev.* **2010**, *110*, 389–458.
[2] E. H. Sargent, *Adv. Mater.* **2008**, *20*, 3958–3964.
[3] J. Tang, X. Wang, L. Brzozowski, D. A. R. Barkhouse, R. Debnath, L. Levina, E. H. Sargent, *Adv. Mater.* **2010**, *22*, 1398–1402.
[4] J. M. Luther, M. Law, M. C. Beard, Q. Song, M. O. Reese, R. J. Ellingson, A. J. Nozik, *Nano Lett.* **2008**, *8*, 3488–3492.
[5] I. Moreels, K. Lambert, D. Smeets, D. De Muynck, T. Nollet, J. C. Martins, F. Vanhaecke, A. Vantomme, C. Delerue, G. Allan, Z. Hens, *ACS Nano* **2009**, *3*, 3023–3030.

[6] K.-S. Cho, D. V. Talapin, W. Gaschler, C. B. Murray, *J. Am. Chem. Soc.* **2005**, *127*, 7140–7147.
[7] T. Hanrath, D. Veldman, J. J. Choi, C. G. Christova, M. M. Wienk, R. A. J. Janssen, *ACS Appl. Mater. Interfaces* **2009**, *1*, 244–250.
[8] C.-Y. Kuo, M.-S. Su, C.-S. Ku, S.-M. Wang, H.-Y. Lee, K.-H. Wei, *J. Mater. Chem.* **2011**, *21*, 11605–11612.
[9] D. V. Talapin, C. B. Murray, *Science* **2005**, *310*, 86–89.
[10] M. Law, J. M. Luther, Q. Song, B. K. Hughes, C. L. Perkins, A. J. Nozik, *J. Am. Chem. Soc.* **2008**, *130*, 5974–5985.
[11] S. W. Tsang, H. Fu, R. Wang, J. Lu, K. Yu, Y. Tao, *Appl. Phys. Lett.* **2009**, *95*, 183505.
[12] J. J. Choi, J. Luria, B.-R. Hyun, A. C. Bartnik, L. Sun, Y.-F. Lim, J. A. Marohn, F. W. Wise, T. Hanrath, *Nano Lett.* **2010**, *10*, 1805–1811.
[13] E. J. D. Klem, D. D. MacNeil, P. W. Cyr, L. Levina, E. H. Sargent, *Appl. Phys. Lett.* **2007**, *90*, 183113.
[14] M. H. Zarghami, Y. Liu, M. Gibbs, E. Gebremichael, C. Webster, M. Law, *ACS Nano* **2010**, *4*, 2475–2485.
[15] Y. Liu, M. Gibbs, J. Puthussery, S. Gaik, R. Ihly, H. W. Hillhouse, M. Law, *Nano Lett.* **2010**, *10*, 1960–1969.
[16] J.-S. Lee, M. V. Kovalenko, J. Huang, D. S. Chung, D. V. Talapin, *Nat. Nanotechnol.* **2011**, *6*, 348–352.
[17] J. M. Luther, M. Law, Q. Song, C. L. Perkins, M. C. Beard, A. J. Nozik, *ACS Nano* **2008**, *2*, 271–280.
[18] M. S. Kang, A. Sahu, D. J. Norris, C. D. Frisbie, *Nano Lett.* **2010**, *10*, 3727–3732.
[19] J. Tang, L. Brzozowski, D. A. R. Barkhouse, X. Wang, R. Debnath, R. Wolowiec, E. Palmiano, L. Levina, A. G. Pattantyus-Abraham, D. Jamakosmanovic, E. H. Sargent, *ACS Nano* **2010**, *4*, 869–878.
[20] A. Olkhovets, R.-C. Hsu, A. Lipovskii, F. W. Wise, *Phys. Rev. Lett.* **1998**, *81*, 3539.
[21] H. Ichida, K. O. Mizoguchi, D. Kim, T. Kuwabara, M. Nakayama, *J. Lumin.* **2006**, *119*, 457–461.
[22] V. Rinnerbauer, H.-J. Egelhaaf, K. Hingerl, P. Zimmer, S. Werner, T. Warming, A. Hoffmann, M. Kovalenko, W. Heiss, G. Hesser, F. Schaffler, *Phys. Rev. B* **2008**, *77*, 085322.
[23] W. Lu, I. Kamiya, M. Ichida, H. Ando, *Appl. Phys. Lett.* **2009**, *95*, 083102.
[24] C. Liu, Y. K. Kwon, J. Heo, *J. Non-Cryst. Solids* **2009**, *355*, 1880–1883.
[25] M. S. Gaponenko, A. A. Lutich, N. A. Tolstik, A. A. Onushchenko, A. M. Malyarevich, E. P. Petrov, K. V. Yumashev, *Phys. Rev. B* **2010**, *82*, 125320.
[26] S. Pichler, T. Rauch, R. Seyrkammer, M. Bo berl, S. F. Tedde, J. Fuürst, M. V. Kovalenko, U. Lemmer, O. Hayden, W. Heiss, *Appl. Phys. Lett.* **2011**, *98*, 053304.
[27] R. Dalven, in *Solid State Physics: Advancesin Research and Applications*, Vol. 53 (Eds: H. Ehnrenreich, F. Spaepen), Academic Press, San Diego **1999**, pp. 179–224.
[28] K. Szendrei, W. Gomulya, M. Yarema, W. Heiss, M. A. Loi, *Appl. Phys. Lett.* **2010**, *97*, 203501.
[29] K. Sriprapha, I. A. Yunaz, S. Y. Myong, A. Yamada, M. Konagai, *Jpn. J. Appl. Phys.* **2007**, *46*, 7212–7216.
[30] E. A. Katz, D. Faiman, S. M. Tuladhar, J. M. Kroon, M. M. Wienk, T. Fromherz, F. Padinger, C. J. Brabec, N. S. Sariciftci, *J. Appl. Phys.* **2001**, *90*, 5343.
[31] W. Bagienski, M. C. Gupta, *Sol. Energy Mater. Sol. Cells* **2011**, *95*, 933–941.
[32] S. M. Sze, K. K. Ng, *Physics of Semiconductor Devices*, John Wiley And Sons, Hoboken, NJ **2007**.
[33] J. P. Clifford, K. W. Johnston, L. Levina, E. H. Sargent, *Appl. Phys. Lett.* **2007**, *91*, 253117.
[34] A. Assadi, C. Svensson, M. Willander, O. Inganaäs, *J. Appl. Phys.* **1992**, *72*, 2900.
[35] J. Gao, J. M. Luther, O. E. Semonin, R. J. Ellingson, A. J. Nozik, M. C. Beard, *Nano Lett.* **2011**, *11*, 1002–1008.
[36] N. I. Craciun, J. Wildeman, P. W. M. Blom, *Phys. Rev. Lett.* **2008**, *100*, 056601.
[37] A. J. Houtepen, D. Kockmann, D. Vanmaekelbergh, *Nano Lett.* **2008**, *8*, 3516–3520.
[38] H. Liu, A. Pourret, P. Guyot-Sionnest, *ACS Nano* **2010**, *4*, 5211–5216.
[39] H. S. Nalwa, *Handbook of Thin Film Materials: Nanomaterials and Magnetic Thin Films*, Academic Press, San Diego **2002**.
[40] K. Tamura, K. Hirakawa, Y. Shimada, *Physica B: Condensed Matter* **1999**, *272*, 183–186.
[41] G. Markovich, C. P. Collier, S. E. Henrichs, F. Remacle, R. D. Levine, J. R. Heath, *Acc. Chem. Res.* **1999**, *32*, 415–423.
[42] J. M. Harbold, F. W. Wise, *Phys. Rev. B* **2007**, *76*, 125304.
[43] V. Rinnerbauer, H.-J. Egelhaaf, K. Hingerl, P. Zimmer, S. Werner, T. Warming, A. Hoffmann, M. Kovalenko, W. Heiss, G. Hesser, F. Schaffler, *Phys. Rev. B* **2008**, *77*, 085322.
[44] A. Wolcott, V. Doyeux, C. A. Nelson, R. Gearba, K. W. Lei, K. G. Yager, A. D. Dolocan, K. Williams, D. Nguyen, X.-Y. Zhu, *J. Phys. Chem. Lett.* **2011**, *2*, 795–800.
[45] S. F. Wuister, A. van Houselt, C. de Mello Donegá, D. Vanmaekelbergh, A. Meijerink, *Angew. Chem. Int. Ed.* **2004**, *43*, 3029–3033.
[46] S. F. Wuister, C. de Mello Donegá, A. Meijerink, *J. Am. Chem. Soc.* **2004**, *126*, 10397–10402.
[47] D. V. Talapin, A. L. Rogach, A. Kornowski, M. Haase, H. Weller, *Nano Lett.* **2001**, *1*, 207–211.
[48] M. Kuno, J. K. Lee, B. O. Dabbousi, F. V. Mikulec, M. G. Bawendi, *J. Chem. Phys.* **1997**, *106*, 9869.
[49] C. de Mello Donegá, S. G. Hickey, S. F. Wuister, D. Vanmaekelbergh, A. Meijerink, *J. Phys. Chem. B* **2003**, *107*, 489–496.
[50] A. M. Kapitonov, A. P. Stupak, S. V. Gaponenko, E. P. Petrov, A. L. Rogach, A. Eychmüller, *J. Phys. Chem. B* **1999**, *103*, 10109–10113.
[51] Y. Nonoguchi, T. Nakashima, T. Kawai, *J. Phys. Chem.C* **2007**, *111*, 11811–11815.
[52] N. B. Pendyala, K. S. R. Koteswara Rao, *J. Lumin.* **2008**, *128*, 1826–1830.
[53] G. W. Bryant, W. Jaskolski, *J. Phys. Chem. B* **2005**, *109*, 19650–19656.
[54] S. W. Clark, J. M. Harbold, F. W. Wise, *J. Phys. Chem. C* **2007**, *111*, 7302–7305.
[55] K. Szendrei, F. Cordella, M. V. Kovalenko, M. Böberl, G. Hesser, M. Yarema, D. Jarzab, O. V. Mikhnenko, A. Gocalinska, M. Saba, F. Quochi, A. Mura, G. Bongiovanni, P. W. M. Blom, W. Heiss, M. A. Loi, *Adv. Mater.* **2009**, *21*, 683–687.
[56] F. Xu, X. Ma, C. R. Haughn, J. Benavides, M. F. Doty, S. G. Cloutier, *ACS Nano* **2011**, DOI 10.1021/nn203728t.
[57] J. H. Warner, E. Thomsen, A. R. Watt, N. R. Heckenberg, H. Rubinsztein-Dunlop, *Nanotechnology* **2005**, *16*, 175–179.